Eur Biophys J (2004) 33: 477–489
DOI 10.1007/s00249-004-0398-z

ARTICLE

Richard J. Law · Mark S. P. Sansom

Homology modelling and molecular dynamics simulations: comparative studies of human aquaporin-1

Received: 18 November 2003 / Revised: 10 February 2004 / Accepted: 12 February 2004 / Published online: 8 April 2004

Abstract The structures of the mammalian water transport protein Aqp1 and of its bacterial homologue GlpF enables us to test whether homology models can be used to explore relationships between structure, dynamics and function in mammalian transport proteins. Molecular dynamics simulations (totalling almost 40 ns) were performed starting from: the X-ray structure of Aqp1; a homology model of Aqp1 based on the GlpF structure; and intermediate resolution structures of Aqp1 derived from electron microscopy. Comparisons of protein RMSDs vs. time suggest that the homology models are of comparable conformational stability to the X-ray structure, whereas the intermediate resolution structures exhibit significant conformation drift. For simulations based on the X-ray structure and on homology models, the flexibility profile vs. residue number correlates well with the crystallographic B-values for each residue. In the simulations based on intermediate resolution structures, mobility of the highly conserved NPA loops is substantially higher than in the simulations based on the X-ray structure or the homology models. Pore radius profiles remained relatively constant in the X-ray and homology model simulations but showed substantial fluctuations (reflecting the higher NPA loop mobility) in the intermediate resolution simulations. The orientation of the dipoles of water molecules within the pore is of key importance in maintaining low proton permeability through Aqp1. This property seems to be quite robust to the starting model used in the simulation. These simulations suggest that homology models based on bacterial homologues may be used to derive functionally relevant information on the structural dynamics of mammalian transport proteins.

Keywords Aquaporin · Membrane protein · Homology model · MD simulation

R. J. Law · M. S. P. Sansom (✉)
Laboratory of Molecular Biophysics,
Department of Biochemistry,
The University of Oxford,
South Parks Road,
Oxford, OX1 3QU, UK
E-mail: mark.sansom@biop.ox.ac.uk
Tel.: +44-1865-275371
Fax: +44-1865-275182

Present address: R. J. Law
Chemistry and Biochemistry Dept.,
University of California,
San Diego, 9500 Gilman Drive,
La Jolla, CA 92093–0365, USA

Introduction

The aquaporins (Aqps) are a family of integral membrane proteins responsible for rapid (ca. 10^9 molecules·s^{-1}) passive transport of water across membranes (Borgnia et al. 1999; Fujiyoshi et al. 2002). Over 200 aquaporin sequences have been found from a wide range of organisms (Hohmann et al. 2000). Phylogenetic analysis allows these to be divided into the aquaporins, which are strictly water selective, and the glyceroaquaporins, which in addition to water are also permeable to small neutral solutes, such as glycerol (Park and Saier 1996). Water transport through aquaporins is highly selective. Ions, including protons, cannot pass through the aquaporin pore.

The Aqp sequence exhibits internal twofold symmetry. This combined with topological analysis resulted in the proposal of an 'hourglass' model (Heymann and Engel 2000) for the Aqp monomer, which was subsequently confirmed by the X-ray structures of bovine Aqp1 (Sui et al. 2001) and of a bacterial glyceroaquaporin GlpF (Fu et al. 2000). Aqp1 is functional as a tetramer (Verbavatz et al. 1993) with a pore at the centre of each monomer. The structure of the Aqp monomer mirrors the twofold symmetry seen in its sequence—it is composed of a repeated motif containing three transmembrane helices and a re-entrant loop that contains a helix that half-spans the membrane plus a conserved NPA motif. The conserved NPA motifs contribute to a selectivity filter in the middle of the pore. A second

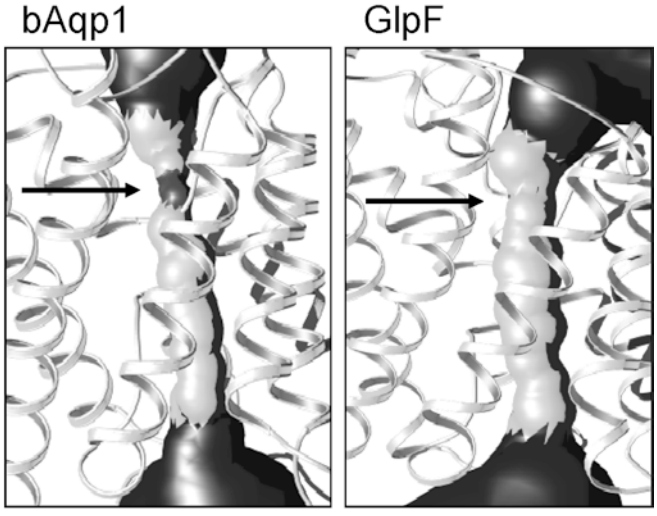

Fig. 1 Comparison of pore-lining surfaces (calculated using HOLE; Smart et al. 1996) of bovine Aqp1 (1j4n) and *E. coli* GlpF (1fx8). The extracellular end of the pore is uppermost. *Arrows* indicate the restriction site, i.e. the narrowest region of each pore

region of the structure important for selectivity is the restriction site (the narrowest section of the pore), located in the upper (i.e. extracellular) half of the pore (Fig. 1). This region is slightly wider in GlpF to allow the passage of a glycerol molecule (de Groot and Grubmuller 2001; Fu et al. 2000).

There are several entries for aquaporins in the protein databank (Table 1; http://www.rcsb.org). These include medium resolution models from electron microscopy (EM) (1ih5; 1fqy), EM structures refined by further model building (1h6i) and high resolution X-ray structures for bovine Aqp1 (1j4n) and for its bacterial homologue GlpF (1fx8). Having the structure of a mammalian membrane protein by both X-ray diffraction and EM *and* high resolution structures of both a mammalian membrane protein and one of its bacterial homologues provides us with a nearly unique opportunity to evaluate different approaches to membrane protein structural biology. In particular, it provides a test case to explore to what extent one may extrapolate from the structure of bacterial homologues and/or low resolution models from EM to a high resolution model of a mammalian protein that can be employed in simulation studies. Such simulation studies have already provided considerable insights into the functional dynamics of Aqp1 (de Groot et al. 2003; de Groot and Grubmuller 2001). and GlpF (Jensen et al. 2001; Tajkhorshid et al. 2002; Zhu et al. 2001).

The major aim of the current study is use molecular dynamics (MD) simulations to compare the structural stability of the different models of Aqp1 and to determine the extent to which key functional aspects of the simulation results are robust to changes in the protein model. This is important in the context of using bacterial transport protein and channel structures as templates for homology models of mammalian proteins. For example, the recent structures of lactose permease (Abramson et al. 2003) and of the glycerol-3-phosphate transporter GlpT (Huang et al. 2003) provide possible templates for modelling mammalian sugar and related transporters, and the structures of KirBac (Kuo et al. 2003) and of KvAP (Jiang et al. 2003) provide templates for mammalian inward rectifier and voltage-gated potassium channels, respectively. However, it remains an important issue to determine the extent to which homology models of mammalian transporters and channels may be used in analysis of structure/function relationships. The aquaporin family provides a good opportunity to further explore this issue as high resolution structures are known for both a bacterial (GlpT) and a mammalian (Aqp1) homologue. In particular, we have focused on the ability to explain key functional aspects of Aqp function, namely the mechanisms of selection for water permeation and against proton conduction, on the basis of different structural models.

Table 1 Aquaporin structures used in simulations

Protein	Structure	Reference	Source	Resolution (Å)
hAqp1	1ih5	Ren et al. (2001)	EM	3.7
hAqp1	1ih5ref[a]	Ren et al. (pers. comm.)	EM	3.7
hAqp1	1fqy	Murata et al. (2000)	EM	3.8
hAqp1	1h6i[b]	de Groot et al. (2001)	EM/homology	3.8
bAqp1	1j4n	Sui et al. (2001)	X-ray	2.2
hAqp1	hMod	Law (this paper)	Homology	-
AqpZ	zMod	Law (this paper)	Homology	-

[a]A refinement of the previous model (1ih5)
[b]A refined version of 1fqy, including data from the GlpF (1fx8) structure

Materials and methods

System preparation

Homology modelling used Modeller v4.0 (Sali and Blundell 1993; http://www.salilab.org/modeller/modeller.html) with the 2.2-Å resolution structure of GlpF (1fx8) (Fu et al. 2000) as a template. Fourfold symmetry was imposed when modelling the tetramer structure. Sequence alignments for input to modelling were generated using ClustalW in Jalview (http://www.ebi.ac.uk:80/jalview/index.html). Structures and models were checked and compared using Procheck (Laskowski et al. 1993), Prove (Pontius et al. 1996) and Whatcheck (Rodriguez et al. 1998). Prior to running simulations, sidechain ionisation states were adjusted to match the results of pK_A calculations, performed as described in (Adcock et al. 1998), using UHBD (Davis et al. 1991) to calculate free energy differences between ionised and unionised sidechains of the protein. Protonation states were then checked manually to assure no inappropriate

results due to the approximations of the method (Nielsen 2003), and the H-bonding network was not optimised prior to the calculation.

For the comparative simulations, each model/structure was embedded in a membrane mimetic octane slab (Capener and Sansom 2002; Tieleman et al. 2001a) and the system was then solvated with SPC (Hermans et al. 1984; van Gunsteren et al. 1996) waters. The MMC method (Resat and Mezei 1996; http://inka.mssm.edu/~mezei/mmc/) was used to place waters in the pores of aquaporin models. This yielded ca. 12 water molecules within the central 20 Å section of each pore. Counterions were added to yield an electroneutral system that was energy minimized prior to starting simulations (Fig. 2).

Simulations

Simulations were performed as described in earlier papers (Forrest et al. 2000; Law et al. 2000; Tieleman et al. 1999) using NPT and periodic boundary conditions. A constant pressure of 1 bar was applied independently in all three directions, using a coupling constant of $\tau_P = 1.0$ ps. Water, octane and protein were coupled separately to a temperature bath at 300 K using a coupling constant $\tau_T = 0.1$ ps (Berendsen et al. 1984). Long-range interactions were dealt with using a twin-range cut-off: 10 Å for van der Waals interactions; and 17 Å for electrostatic interactions. Electrostatics treatments were compared by using particle-mesh Ewald (PME; Darden et al. 1993) for some simulations. The time step was 2 fs, using LINCS (Hess et al. 1997) to constrain bond lengths, and the force field was based on GROMOS 87 (Hermans et al. 1984). Prior to the production run, for each system, a 0.5 ns equilibration simulation was conducted, with the position of the non-hydrogen protein atoms restrained with a force constant of 1,000 kJ·mol^{-1} nm^{-2}. This was to enable the water and octane to pack around the protein.

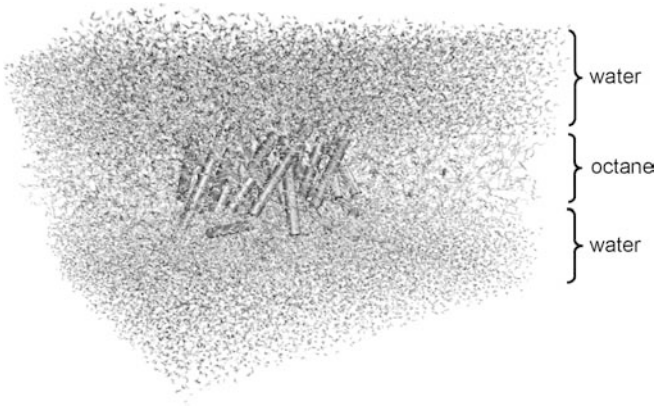

Fig. 2 An example of a simulation system used in this study. The protein (here the bXray$_4$ tetramer) is at the centre of the box with the α-helices drawn as *cylinders*. It is embedded in a slab of octane molecules with waters on either side. For this simulation (bXray$_4$), the box size is 140×140×100 Å

Computational details

Simulations and analysis were carried out using GROMACS v2.0 (Berendsen et al. 1995; http://www.gromacs.org). MD simulations were run on a linux cluster of 64×750 Mhz, Pentium III processors. Simulation times were ~10 days/ns on eight nodes, for the tetramer, and 2 days/ns on eight nodes, for the monomer simulations. Electrostatics calculations for pK_A calculations employed a modified version of UHBD v.5.1 (Davis et al. 1991; http://chemcca51.ucsd.edu/uhbd.html). Pore radius profiles were calculated using HOLE (Smart et al. 1993). Structures were examined using Quanta (Accelrys) and RasMol (Sayle and Milner-White 1995). Molecular graphics images were prepared using VMD (Humphrey et al. 1996), Molscript (Kraulis 1991) and Povray (http://www.povray.org).

Results

Models used and simulations performed

A major aim of this study was to explore a range of aquaporin models of differing levels of accuracy and refinement with respect to their behaviour in 2–5 ns duration MD simulations. To this end, we explored models ranging from EM models based on data at ca. 3.8 Å resolution to X-ray structures at 2.2 Å resolution and also included homology models of human Aqp1 and *E. coli* AqpZ based on the structure of the *E. coli* homologue GlpF (Tables 1 and 2). Note that the EM structures of hAqp1 include one, deGMod, for which the crystal structure of GlpF had been used to aid the modelling and interpretation of the EM data. The models were all quite similar—with their Cα positions not differing from each other, or the X-ray structure, by more than 3 Å.

A summary of the simulations performed is provided in Table 2. Note that this corresponds to a total simulation time of ca. 37 ns. All of the structures/models have been used as the starting point for simulations of the monomeric protein with longer-range electrostatics approximated via a cut-off. The simulations of monomeric RenEM and hMod were also performed using PME to treat long-range electrostatics. The intention behind this was to explore the effect of cut-off vs. PME on simulation stability as a number of studies of simpler systems (Tieleman et al. 2002; Tobias 2001) have suggested that the treatment of electrostatics may have a significant effect. Three of the structures/models (ReEM, bXray and hMod) were also selected to simulate Aqp1 in the tetrameric form. Here, the intention was to explore the relative conformational stability, on a

Table 2 Simulations performed. Number of counterions = 4 Cl^- per monomer, except for bXray which needed 7 Cl^- per monomer. Number of waters = 12,000 for monomer simulations; 42,000 for tetramer simulations. Number of octanes = 650 for monomer simulations; 2,100 for tetramer simulations

Simulation	Structure	Long-range electrostatics	RMSD at 2 ns (Å)[a]	Total duration (ns)
Monomer				
RenEM	1ih5	cut-off	3.1	2
$RenEM_{PME}$	1ih5	PME	3.0	2
RenEMref	1ih5ref	cut-off	4.6	2
MurEM	1fqy	cut-off	3.9	2
deGMod	1h6i	cut-off	2.9	5
bXray	1j4n	cut-off	1.8	5
hMod	hMod	cut-off	2.1	5
$hMod_{PME}$	hMod	PME	2.0	5
zMod	zMod	cut-off	3.0	2
Tetramer				
$RenEM_4$	1ih5	cut-off	3.5	2
$bXray_4$	1j4n	cut-off	2.4	3
$hMod_4$	hMod	cut-off	3.1	2

[a] RMSD vs. starting structure of TM helix Cα atoms at 2 ns

nanosecond timescale, of the monomer vs. the (more physiologically relevant) tetramer.

Structural drift

One may use the drift from the initial conformation as a simple measure of the relative 'stability' of a given structure in a simulation. The drift may be measured as the time-dependent Cα atom root mean square deviation (RMSD) from the initial structure (Fig. 3). In order to focus on conformational drift involving possible repacking of transmembrane (TM) α-helices, we have restricted our RMSD calculations to those Cα atoms in the TM helices and in the NPA-loops, i.e. the extramembranous loops were excluded from the calculation, as were the 12 residue C-terminal and 9 residue N-terminal tails.

From previous experience with simulations of other membrane proteins (Bond et al. 2002; Bond and Sansom 2003; Capener and Sansom 2002; Shrivastava and Sansom 2000), we anticipated that any substantial conformational drifts (i.e. large jumps in RMSD) would occur during the first couple of nanoseconds for a protein such as Aqp embedded in an octane slab. From the results of the analysis shown in Fig. 3, it is evident that for a number of the simulations the TM Cα RMSD after 2 ns is sufficiently high (i.e. ≥3 Å) to indicate that these models are conformationally unstable, at least in their monomeric state. On this basis, only four of the nine simulations (namely deGMod, hMod, $hMod_{PME}$ and bXray) were extended to 5 ns.

A key finding emerges from this simple analysis, namely that hMod seems to be significantly more conformationally stable than MurEM and RenEM, i.e. the two 'raw' EM structures. Not surprisingly, the X-ray

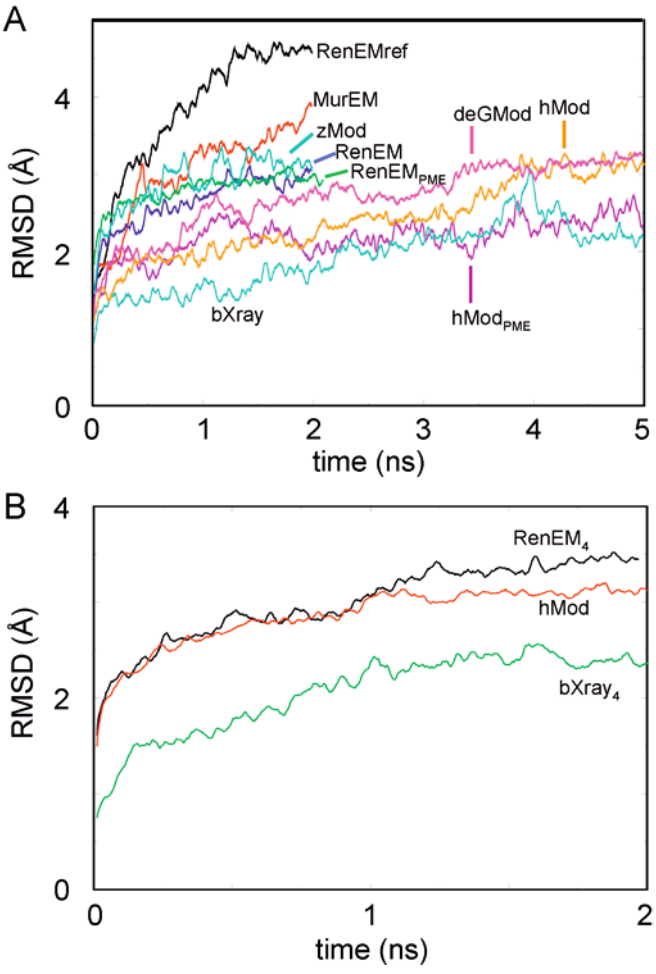

Fig. 3 RMSDs relative to the initial structures of TM helix Cα atoms for simulations of **A** monomers and **B** tetramers

structure of bAqp1 (bXray) is the most stable. Significantly, both hMod and deGMod (which included information from the GlpF structure) were of intermediate stability. Thus, it seems that a ~2 ns simulation is sufficient to establish whether a model is unstable. However, over this duration of simulation we did not observe convergence (as measured by Cα RMSD matrices, data not shown) of, e.g., the homology model and intermediate resolution structures either with one another or with the X-ray structure.

It is also of interest that at 2 ns there was no major difference between the RMSDs of the RenEM and $RenEM_{PME}$ simulations, nor between hMod and $hMod_{PME}$. This suggested that the simulation results were not overly sensitive to the simulation conditions, even though Aqp1 has a significant molecular dipole (de Groot and Grubmuller 2001) and thus might be expected to be influenced by longer range electrostatics (Tieleman et al. 2002). On this basis, most of the longer simulations used a cut-off, although $hMod_{PME}$ was also extended to 5 ns for completeness of comparison.

Secondary structure analysis (using DSSP; Kabsch and Sander 1983) of all of the simulated structures/

models showed that the initial secondary structure was largely retained throughout the simulations (results not shown). There was some limited loss of α-helical structure at the termini of the less stable models (RenEM and MurEM). Thus, the majority of the differences in TM Cα RMSDs discussed above lie in differences in the stability of inter-helix packing, rather than in differences in intra-helix stability.

Tetramer vs. monomer

Comparison of the structural drift for the three tetrameric models simulated (Fig. 3B) suggests that bXray (the X-ray structure) is more stable than both RenEM and the homology GlpF-based model hMod. The final Cα RMSD for the bXray tetramer is comparable to that seen for other ca. 2 Å resolution membrane protein structures simulated under similar conditions, e.g. the K channel KcsA (Charlotte Capener, personal communication) or the bacterial outer membrane protein OmpA (Bond et al. 2002).

Although the unit for water conduction is the monomer, aquaporin is functional only as a tetramer (Verbavatz et al. 1993). Thus, it was of interest to examine the degree of stabilization of a structure that resulted occurs from placement of each monomer within a tetrameric assembly. This was measured in terms of:

$$\Delta C\alpha RMSD = \left(\frac{1}{4}\sum_{i} C\alpha RMSD_i\right) - C\alpha RMSD_{mono}$$

where the summation across *i* is for each monomer in the tetramer simulation. It was found that the RenEM model is slightly more stable as a tetramer than a monomer. In contrast, neither hMod or bXray (the X-ray structure) was any more stable as a tetramer than as a monomer. This suggests that assessment of structural stability based on monomer simulations is a reasonable criterion for selecting between the different aquaporins models.

Structural fluctuations

A more detailed comparison of the location of mobile vs. static regions within the aquaporin fold can be provided by the root mean square fluctuations (RMSFs) of Cα atoms as a function of residue number. Such a comparison of the hMod and bXray simulations is informative (Fig. 4) as both of these simulations yielded low conformational drift over the course of 5-ns simulations.

Inspection of the RMSF profiles reveals that the more substantial motions seen in the monomer simulations occur mainly in the extra-membranous loops. The fluctuation profiles for the homology model, hMod, and for the X-ray crystal structure, bXray, are very similar. Noticeably, the magnitude of the TM helix and of the NPA loop fluctuations are very similar in these two simulations. Furthermore, the mobility profile in the bXray simulation correlates well with the corresponding profile of crystallographic B-values of the X-ray structure. The major differences between the simulation RMSFs and the B-values are for the loop between M4 and M5. Interestingly, in both simulations the mobility of this loop is high relative to the crystallographic B-value. The stability of this loop could be affected by being packed within the tetramer, as it contacts the adjacent subunits on the intracellular side of the membrane as well as the structure possibly being affected by the packing within the crystal.

The loop between the TM helices M1 and M2 is very mobile in both of the models and has high B-values in the crystal structure. The long M3-M4 loop, that spans the ''top'' of the channel, is also reasonably mobile, although, in the case of the homology model, it seems to have a more stable region at the centre where it contacts the top of transmembrane helix M5 and the HE as it crosses the top of the channel. It is noticeably more stable in the bXray simulation. Residues at the top of the HE loop form one side of the restriction site, which is different between GlpF and Aqp1, and also form part of the pore lining in both structures. The structure of this long M3-M4 loop is therefore vital in the functional stability of this region. Neither for the EM models nor for the homology model is this loop accurately defined, as demonstrated by its high mobility in simulations.

An extra-membranous tail segment is seen at the C-terminus of the X-ray crystal structure (1j4n) (Sui et al. 2001). This segment contains a series of lysine residues and forms a short helix. It is very mobile in simulation bXray, again matching the B-values. There are a further 22 residues in the C-terminus of the Aqp1 sequence that were not resolved in the X-ray structure.

NPA loop motions

From the perspective of using simulations and models to understand biological function, the conformational stability of the structures/models is important because it relates directly to the geometry and electrostatics of the water permeable pore. Of especial importance in this respect are the NPA loops, both of which make major contributions to the lining of the pore. These loops lie adjacent to the pore, and their residues may have several roles in the water selection and transport process.

For each of the simulations, the structural drift of the NPA loops (HB and HE) was determined as a function of time (Fig. 5). In previously published simulations based on the EM structures (Zhu et al. 2001), the NPA loops had to be restrained to prevent their motion from blocking the pore-to-water passage, yet for comparable simulations of GlpF (de Groot and Grubmuller 2001; Tajkhorshid et al. 2002), the NPA loops appeared to be much less flexible. The structural drift in the NPA loops broadly followed the patterns in RMSDs seen for the whole TM structures. In particular, the NPA loops in the medium resolution EM structures (RenEM and

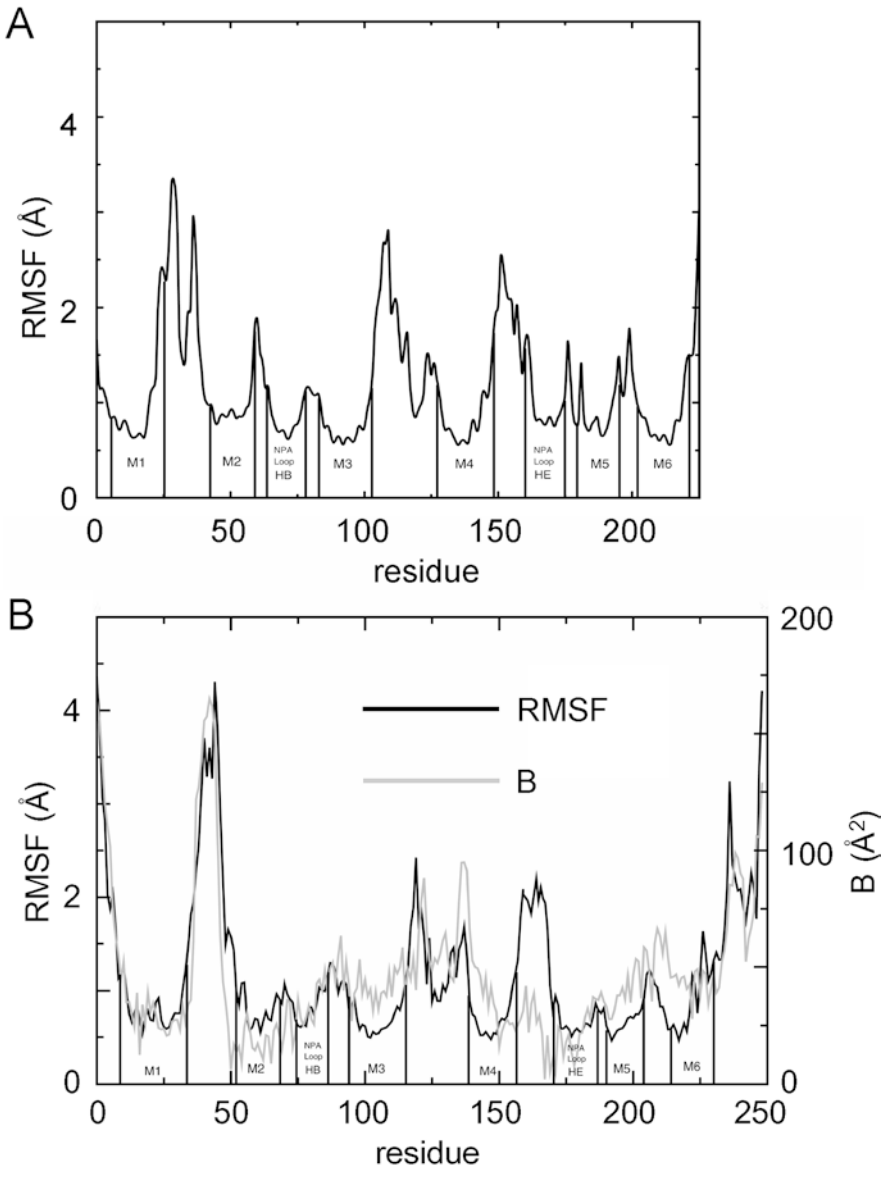

Fig. 4 Root mean square fluctuation about the average positions of the Cα atoms in **A** the homology model and **B** the bXray monomer simulation as a function of residue number compared with crystallographic B-value in the 1j4n X-ray structure of bAqp1

MurEM) underwent a substantial (RMSD ~3 Å) conformational change within ca. 0.5 ns and appeared to be too mobile to allow a stable column of water to remain in the channel, the loop mobility having the effect of closing the pore (Fig. 6). In the simulations of the homology model (hMod), the EM model refined against GlpF (deGMod) and the X-ray structure (bXray), these NPA loops were seen to be much more stable, even on a 5 ns timescale. Indeed, the magnitude of the fluctuations in NPA loop conformation in these simulations was similar to that of the TM helices. The relative rigidity of the selectivity loops in e.g. deGMod (Fig. 6) was mirrored in the stability of the pore geometry (see below).

Pore and water properties

Having compared the conformational stabilities of the different models we examined some of the functionally relevant properties of the pore and the water molecules within it, and explored how robust these properties are to changes in model and simulation conditions.

Pore radius profiles

The pore radius profiles of the various aquaporin structures/models are remarkably similar prior to simulation. All of the structures/models have a pore radius profile capable of accommodating only a single file column of water. The restriction sites, lined by R195 and F56, were seen to be very similar in each initial model. Of course, this site is different in the GlpF structure where it is slightly wider to allow the passage of a glycerol molecule.

In contrast, the dynamic fluctuations in the pore radius profiles during the simulations revealed significant differences in behaviour between the different models

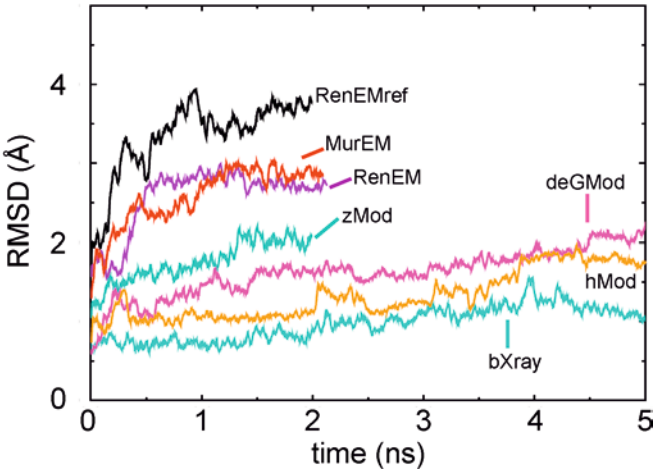

Fig. 5 RMSDs of Cα atoms of the NPA loops (defined as residues S73-L86 and T184-S202, and fitted to the NPA loops prior to calculation of RMSDs) for monomer simulations using cut-off electrostatics

(Fig. 7). The differences in pore radius profiles parallel the differences in structural drift and in mobility of the NPA loops. The less stable models (i.e. RenEM, RenEMref, and MurEM) exhibit much larger fluctuations in their pore radii, especially at the location of the

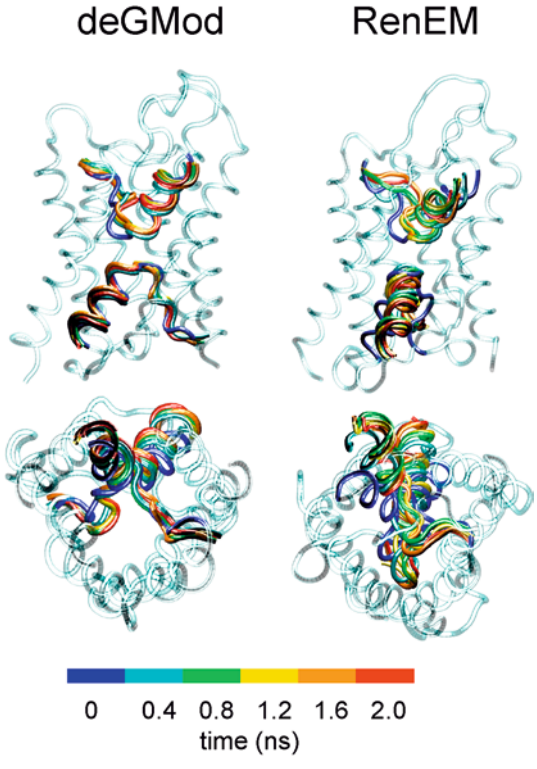

Fig. 6 NPA loop motion compared in monomer simulations: deGMod (similar in behaviour to simulations bXray and hMod) and RenEM (similar in behaviour to simulations RenEMref and MurEM). The *upper diagrams* are viewed perpendicular to the pore axis (extracellular mouth uppermost); the *lower diagrams* are viewed down the pore axis from the intracellular mouth. Snapshots of the loops every 0.4 ns during a 2-ns period are coloured on a blue to red scale

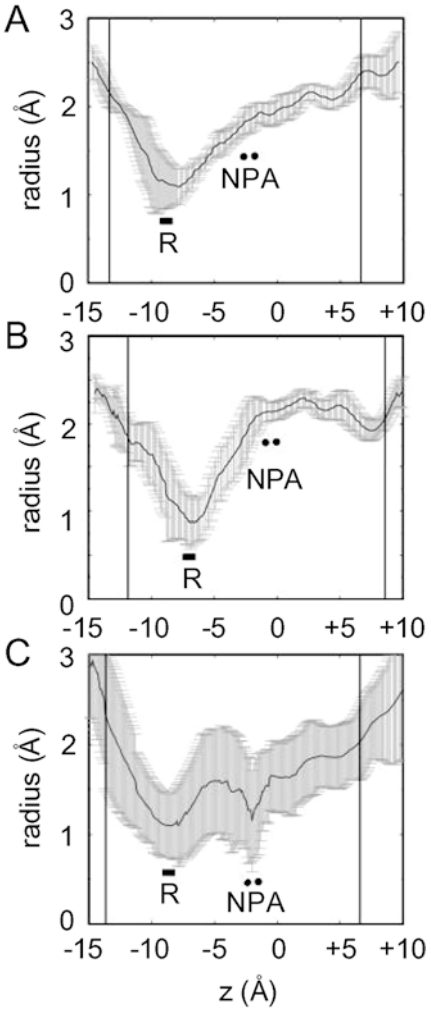

Fig. 7 Pore radius profiles for **A** tetramer simulation $bXray_4$, **B** monomer simulation bXray, and **C** tetramer simulation $RenEM_4$. In each plot, the line represents the radius averaged over the whole simulation (*error bars* are ±SD). The *vertical lines* represent the boundaries of the pore at the extracellular mouth (z ca. −12 Å) and the intracellular mouth (z ca. +7 Å). *Filled circles* show the position of the NPA motifs at the centre of the pore, and the *bar* show the restriction site (*R*)

two NPA motifs, and these fluctuations generally serve to constrict and block the pore. In contrast, bXray, de GMod, and hMod exhibit relatively small fluctuations in pore radius, allowing a stable column of water molecules to remain within the pore. The average pore radius is only reduced below the radius of a water molecule at the restriction site. However, dynamic fluctuations are such as to allow a single water molecule to pass this apparent barrier. A comparable effect is seen in the selectivity filter of K channels (Bernèche and Roux 2001). In all the models, the channel is too narrow in the vicinity of restriction site to accommodate a Cl^- ion (radius 1.81 Å), even though the positive potential at the centre of the pore might suggest that this would be possible.

A comparison of the pore radius profile dynamics results for the bXray tetramer (Fig. 7A) and bXray monomer (Fig. 7B) simulations confirms that there is

little difference in the channel geometry between the simulations of the two oligomeric forms of the protein.

Water trajectories

A key biological function of aquaporins is to enable rapid passage of water through the pore without allowing the transport of protons (or hydroxonium ions). Recent structural (Sui et al. 2001) and simulation (de Groot and Grubmuller 2001) studies have focused attention on two sites, the constriction site (Fig. 1) and the centre of the pore where the paired NPA motifs are located. The constriction site can generate transient breaks in the single file column of waters within the pore (Fig. 8), i.e. the H-bonded chain of waters is broken at this point. During the bXray, deGMod, hMod, $bXray_4$, and $hMod_4$ simulations, the waters in the aquaporin pore show mostly single filing activity, yet several crossing events were also observed, reflecting the small fluctuations in geometry of the pore.

Most of the residues lining the aquaporin pore are hydrophobic. However, the backbone carbonyls exposed to the pore provide up to eight H-bond accepters, and the central asparagine side chains of the NPA motifs provide two H-bond donors to a central water molecule (Fig. 9). At the restriction site, the H-bonding between waters is often broken. This requires an extra H-bond donor and acceptor. The histidine residue, H180 (which is completely conserved amongst water selective aquaporins; Heymann and Engel 2000), seems to provide the role of the acceptor. On the other side of the restriction site, R197 is in position to act as the extra H-bond donor.

The carbonyl oxygens and the two asparagines from the NPA loops all occupy the same side of a helical pathway through the pore. The other side of the pathway is lined by hydrophobic residues, such as F26 (opposite the central asparagines), F58 (at the restriction site), I174, L151, and Y229 (both in the cytoplasmic half of the channel). The arrangement of all these pore-lining residues remains reasonably stable throughout the course of the simulations. However, they do fluctuate in position, and this dynamic behaviour is mirrored in the dynamic nature of the H-bonding network of the pore waters, i.e. not all of the single-file water H-bonds are satisfied at all times.

Another functionally important aspect of water within the aquaporins pore, already stressed by a number of authors (e.g. de Groot and Grubmuller 2001; Tajkhorshid et al. 2002), is the reversal of water dipole orientations as the water molecules move past the central NPA motif site. This is thought to play a central role in preventing proton permeability. This behaviour is illustrated in Fig. 9. A more quantitative comparison of this behaviour in different simulations is provided below.

Water dipole reorientation

As mentioned above, control of the dipole orientation of the single file waters in the pore may play a role in preventing the movement of protons through the

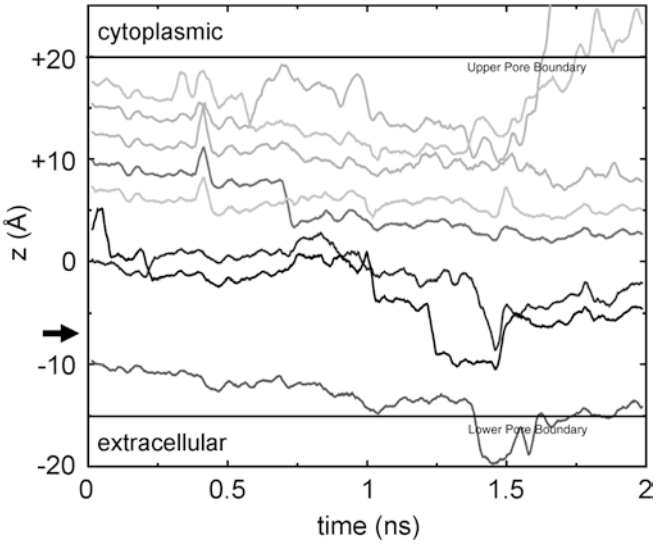

Fig. 8 Trajectories of eight water molecules, present within the pore for greater than 1.5 ns, for one of the pores in the $1jn4_4$ simulation. The positions of the water molecules are projected onto the pore (z) axis. The *arrow* shows the approximate position of the restriction site. Note the break in the single column of water molecules that occurs in the vicinity of the restriction site. This break is quite long-lived. Similar behaviour is seen in the bXray, deGMod, hMod, $bXray_4$, and $hMod_4$ simulations

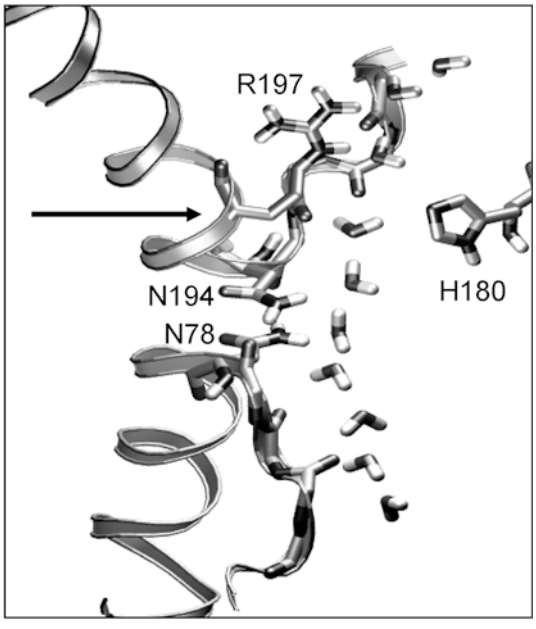

Fig. 9 Snapshot from the bXray simulation at $t = 1$ ns. It illustrates part of the H-bonding network that solvates the single-file column of water in the Aqp1 pore. The side chains of N78 and N194 define the centre of the pore. The restriction site (*horizontal arrow*) and the side chains of H180 and R197 are also indicated

channel (de Groot and Grubmuller 2001; Tajkhorshid et al. 2002). The dipole orientation can be measured as the cosine of the angle (θ) between the water dipole relative and the z-axis, the latter being approximately equivalent to the pore axis. Plotting the simulation average of cosθ as a function of z, we obtain a water dipole profile along the pore (Fig. 10) that reveals quite clearly the reversal in dipole orientation of waters between the extracellular and cytoplasmic halves of the pore. Significantly, if we compare the water dipole profiles for the three simulations (deGMod, hMod, and bXray) for which the structural drift was relatively low, we observe conservation of the overall shape of the water dipole profile. This suggests that this functionally important aspect of water behaviour in aquaporins simulations is robust to small changes in the structure of the model, provided that the model is sufficiently conformationally stable to retain the integrity of the pore.

Recent simulations of e.g. alamethicin channels (Tieleman et al. 2002) have suggested a degree of sensitivity of the dipolar ordering of pore waters to the treatment of long-range electrostatics in the simulations. In particular, significantly different behaviour was seen between those simulations employing a cut-off and those employing PME. However, comparison of the profiles for hMod and hMod_{PME}, whilst revealing some differences in detail, especially at the mouth of the pore and near the water/octane interface, suggest that the treatment of long-range electrostatics in the simulation does *not* significantly alter the water dipole profile in the current system. In the pore, the water orientation is not significantly different for hMod (cut-offs) and hMod_{PME} as the cut-off lengths are long enough (13 Å) that waters at each mouth of the pore can see the pore-helix dipole at the centre. This difference between aquaporins and alamethicin may relate to the rather wider pores (radius 2.5–3 Å) in the latter system. The use of different water forcefields was not investigated here, but previous studies have suggested that SPC water is capable of accurately representing the behaviour investigated in this study (Tieleman, 2002).

Overall, it can be seen that a key functionally important feature of the behaviour of water in aquaporin is conserved between simulations of:

1. a model combining data from EM and from homology modelling (deGMod);
2. a homology model (hMod); and
3. a high resolution X-ray structure (bXray) of Aqp1.

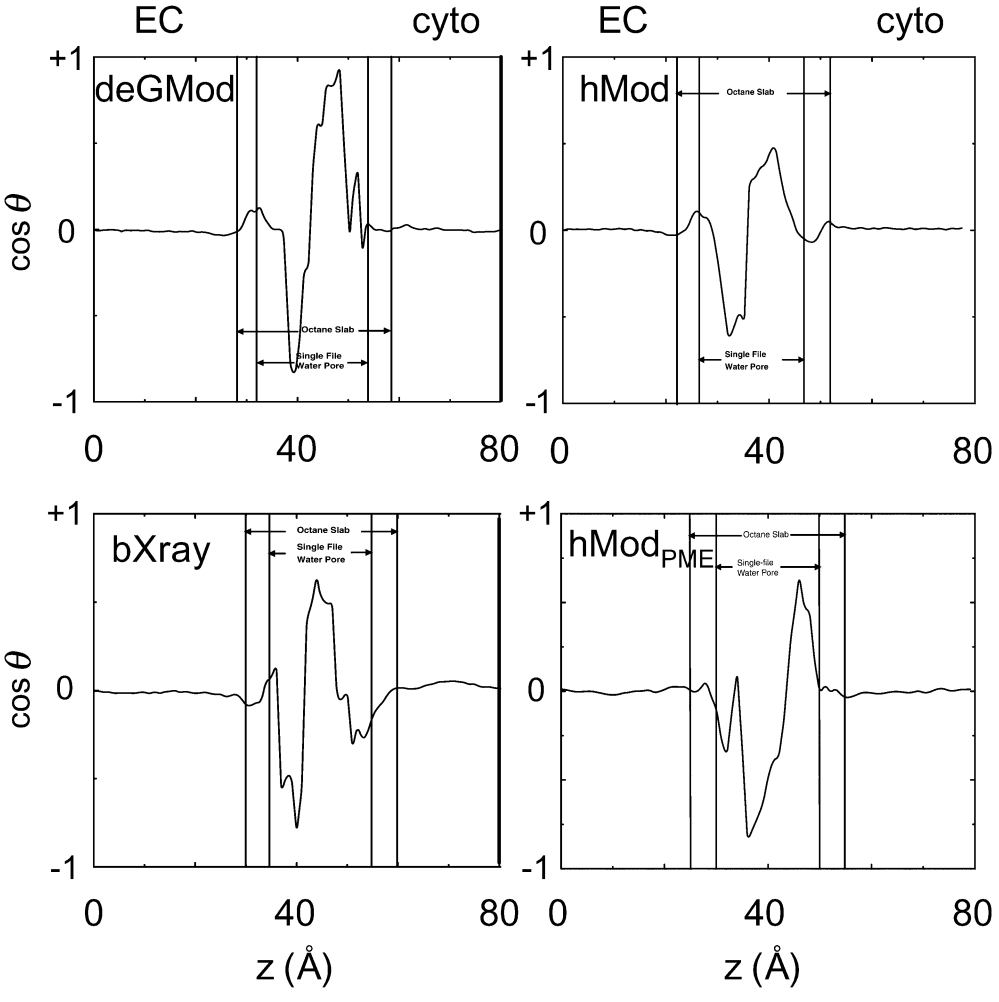

Fig. 10 Water dipole orientations. The average projection of the water dipole onto the pore axis (shown as the average cosine of the angle between the water dipoles and the z axis) is shown as a function of position along the z axis. Results are shown for simulations: deGMod; bXray; hMod (all with cut-off for long-range electrostatics) and hMod_{PME}. The *inner pair of vertical lines* indicates the extent of the single file of water molecules; the *outer pair of vertical lines* indicates the approximate width of the octane slab

Water diffusion

Water diffusion is generally seen to be lower in biological pores than in bulk (Breed et al. 1996; Law et al. 2003; Tieleman et al. 1999; Tieleman et al. 2001b), although there is some evidence (Beckstein and Sansom 2003) that in very hydrophobic pores water self-diffusion rates may be slightly elevated relative to bulk. Given that aquaporin is a water channel and conducts water at near diffusion rates and as its pores are moderately hydrophobic, it was of some interest to investigate water self-diffusion profiles (Fig. 11). It can be seen that within the narrowest central region of the pore the self-diffusion rate along the pore axis is perhaps an order of magnitude lower than in bulk water. The profile shown is for simulation $bXray_4$, but similar profiles were seen for simulations bXray, hMod, $hMod_4$, $hMod_{PME}$, and deGMod, i.e. for those models which were sufficiently conformationally stable for the pore integrity to be maintained during the simulation. Thus, this functionally important property is also robust to changes in the structural model and can be derived from a simulation based on a homology model.

It is noticeable that the water self diffusion coefficient is lower than bulk at some distance from the pore surface. We suspect (based on simple model simulations, Beckstein and Sansom, unpublished results) that this may reflect a degree of ordering of the SPC water at the octane surface. Further studies are needed to elucidate the detailed effects of water model (e.g. SPC vs. SPC/E) and membrane model (e.g. octane vs. phosphatidylcholine) on water dynamics.

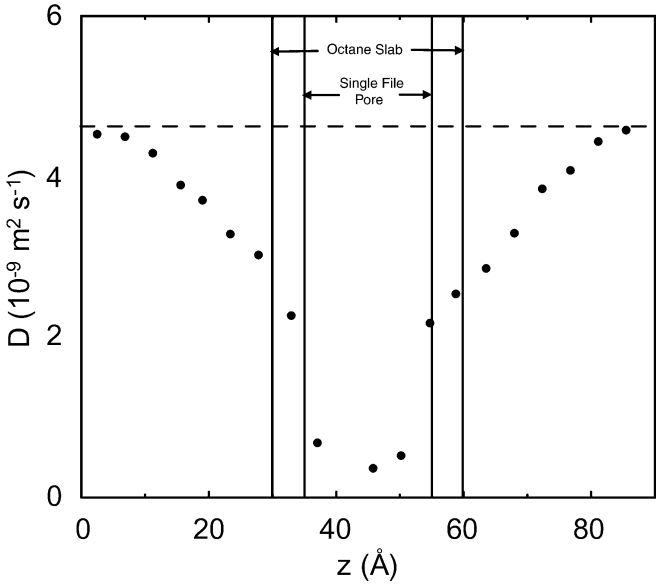

Fig. 11 Average self diffusion coefficients (D) for water molecules in simulation against position along the z axis. The *broken horizontal line* indicates the diffusion coefficient of bulk water in this simulation. The *inner pair of vertical lines* indicates the extent of the single file of water molecules; the *outer pair of vertical lines* indicates the approximate width of the octane slab

Discussion

Model comparisons

A significant finding of this study was that a homology model of Aqp1 (based on GlpF) was more stable in an extended simulation than were the corresponding medium resolution (~3.8 Å) EM structures. Though this is based on a single class of proteins, it provides some encouragement for the use of homology models in simulations designed to explore the role of the conformational dynamics of membrane transport proteins in their physiological function. There have been considerable recent successes in solving X-ray structures of bacterial homologues of mammalian channel and transport proteins (Bass et al. 2002; Chang and Roth 2001; Chang et al. 1998; Doyle et al. 1998; Dutzler et al. 2002; Fu et al. 2000; Jiang et al. 2002; Jiang et al. 2003; Kuo et al. 2003; Locher et al. 2002; Zhou et al. 2001), whereas over-expression of mammalian membrane proteins at a level suitable for X-ray diffraction studies remains somewhat challenging (Tate 2001). Thus, the current demonstration of the value of homology model-based simulations is of particular importance. Whether such homology models will be superior to medium resolution EM-based models for all membrane proteins is less clear. Further studies on a wider range of membrane transport proteins will be required before we can be certain of this.

Methodological aspects: limitations and future directions

Homology modelling is heavily dependent on the quality of the alignment between target and template sequences. Extra-membranous loop regions are often the sites of significant variation in sequences within a family, frequently containing insertions and deletions, thus making the alignment of these regions difficult to optimize (Hein et al. 2000). Furthermore, the conformations of such loops are more difficult to predict than those of the transmembrane segments, and often loops are amongst the least defined regions of a template structure. There are several methods available for more accurate loop modelling (Oliva et al. 1997; Tosatto et al. 2002) including those in newer versions of Modeller (Fiser et al. 2000). The determination of more membrane protein structures should, in due course, provide us with better empirical methods for prediction of loop conformations for this class of protein.

A further limitation of the current study is the use of an approximation to the lipid bilayer environment. An octane slab was used in the current study as a membrane mimetic because its lower viscosity, compared to lipid, allows protein motions to be better sampled over the relatively short timescale of the current MD simulations. However, although octane

may adequately simulate the hydrophobic core of a lipid bilayer, it does not allow for potential interactions of e.g. protein side chains with the polar head-groups of the lipid molecules in a bilayer. In the case of aquaporins, inclusion of lipid head-groups might be anticipated to alter the electrical potential in the interfacial region of the bilayer and, thus, might alter the orientation of water molecules in the mouths of the aquaporin pore (Saiz and Klein 2002).

There are two further limitations to the current study, which may also be of relevance to other modelling and simulation studies of transport proteins. The first is the absence of a transmembrane voltage difference. Such a voltage difference is invariably present across cell membranes but remains difficult to implement in simulations (Roux 1997, 1999). In the context of simulations of Aqp1, it would be of some interest to know whether the transmembrane voltage had any significant effect on the orientation of the water dipoles as they passed through the pore. A further limitation, of key importance to Aqp1 and the question of how H^+ permeation is prevented but also of more general interest to transport protein simulations, is the use of a purely classical model for water and its interactions with the protein. There have been a few ab initio studies of ion channels (e.g. Carloni et al. 2002; Guidoni and Carloni 2002), and empirical models have been used to treat reversible protonation of water molecules (Pomes and Roux 1996, 2002; Schmitt and Voth 1998; Wu and Voth 2002), but further studies are needed in both of these areas.

Biological implications

An important aim of the current study was to further examine the method of selectivity for water of Aqp1 and especially how proton conduction is prevented. Firstly, size selection of water molecules occurs at a constriction site near the extracellular end of the narrow pore, which has a radius of just 1.4 Å. This constriction is ca. 1 Å wider in the equivalent region in GlpF, thus helping to explain how large polar molecules such as glycerol can pass through the GlpF pore but not through Aqp1.

Two of the mechanisms proposed for the prevention of proton wire formation (Murata et al. 2000; Sui et al. 2001) involve specific arrangements of the H-bonding patterns between the waters and the pore lining residues, i.e. H-bonding configurations around the central NPA asparagines and H-bonding of waters to backbone carbonyl atoms of the NPA loop residues (as seen in the bXray structure). Although H-bonding is seen between waters and the NPA loop asparagines, it does not prevent H-bond formation between the waters in the pore. The mutation of several residues, including these asparagines, causes loss or reduction in water transporting capacity of the aquaporins. These mutations are not seen to give rise to the conduction of protons (Jung et al. 1994; Preston et al. 1993). It is therefore likely that these asparagines form part of a network of side chains that provide the exact H-bonding network necessary for the 'solvation' of a fast moving column of water molecules.

The X-ray structure revealed many backbone carbonyl atoms from the NPA loops to point into the pore, and also revealed four electron density peaks assigned to waters. This led to the proposal of a water binding mechanism involving the formation of three 'hydrophilic nodes' (Sui et al. 2001). However, we find little evidence from any of the current simulations that these 'hydrophilic nodes' form preferential binding sites for water. The backbone carbonyls do play a role in satisfaction of water–hydrogen bonds throughout the pore (Fig. 10). The other two structures that were investigated in detail in the current study, 1ih6 and hMod, also had a regular arrangement of backbone carbonyls facing into the pore, which remained available for hydrogen bond acceptance throughout the duration of the simulations.

In those pore-like systems that conduct protons, such as the peptide channel gramicidin (Akeson and Deamer 1991; Pomes and Roux 1996) and the proton pump bacteriorhodopsin (Luecke et al. 1999), 'proton wires' are thought to form so that protons can exchange rapidly via the Grötthuss mechanism. As in the current study, both (de Groot et al. 2003; de Groot and Grubmuller 2001; Tajkhorshid et al. 2002) showed that water molecules in the Aqp1 pore are oriented such that their dipoles point one way in one half of the channel and then have their direction reversed in the other half of the channel due to the the positive electrical field generated by the re-entrant pore helices. As a result of this positive electrostatic potential at the centre of the pore, water dipole orientation constrains the motion of the water molecules to the extent that they cannot re-orientate during a Grötthuss mechanism (Agmon 1995), then proton conduction is unlikely to occur. However, this may not be the sole mechanism preventing proton conduction, as suggested by recent studies (Burykin and Warshel 2003) which favour a simpler electrostatic mechanism of selectivity.

Importantly, the current study shows that several biologically significant observations, such as the role of the NPA loops, of the carbonyl oxygens in the pore and especially of the water dipole orientation, could be observed in a homology model (hMod) and in a low resolution model refined by homology (1ih6), as well as in the high resolution X-ray structure of the channel. Therefore, homology modelling and simulation based on a bacterial transport protein structure can provide meaningful information on the structural dynamics and physiological function of the corresponding mammalian protein.

Acknowledgements Our thanks to Gary Ren and Alok Mitra for providing two of the EM models used in this study and for their continued interest in this work. Our thanks also to George Patargias for discussions concerning GlpF simulations and to our other colleagues for their interest in this work. R.J.L. was supported by an MRC studentship; research in M.S.P.S.'s laboratory is supported by grants from the Wellcome Trust, the BBSRC and the EPSRC. The Oxford Supercomputing Centre provided access to resources.

References

Abramson J, Smirnova I, Kasho V, Verner G, Kaback HR, Iwata S (2003) Structure and mechanism of the lactose permease of *Escherichia coli*. Science 301:610–615

Adcock C, Smith GR, Sansom MSP (1998) Electrostatics and the ion selectivity of ligand-gated ion channels. Biophys J 75:1211–1222

Agmon N (1995) The Grotthuss mechanism. Chem Phys Lett 244:456–462

Akeson M, Deamer DW (1991) Proton conductance by the gramicidin water wire. Biophys J 60:101–109

Bass RB, Strop P, Barclay M, Rees DC (2002) Crystal structure of *Escherichia coli* MscS, a voltage-modulated and mechanosensitive channel. Science 298:1582–1587

Beckstein O, Sansom MSP (2003) Liquid–vapor oscillations of water in hydrophobic nanopores. Proc Nat Acad Sci USA 100:7063–7068

Berendsen HJC, Postma JPM, van Gunsteren WF, DiNola A, Haak JR (1984) Molecular dynamics with coupling to an external bath. J Chem Phys 81:3684–3690

Berendsen HJC, van der Spoel D, van Drunen R (1995) GROMACS: A message-passing parallel molecular dynamics implementation. Comp Phys Comm 95:43–56

Bernèche S, Roux B (2001) Energetics of ion conduction through the K^+ channel. Nature 414:73–77

Bond P, Faraldo-Goméz J, Sansom MSP (2002) OmpA—A pore or not a pore? Simulation and modelling studies. Biophys J 83:763–775

Bond P, Sansom MSP (2003) Membrane protein dynamics vs. environment: simulations of OmpA in a micelle and in a bilayer. J Mol Biol 329:1035–1053

Borgnia M, Nielsen S, Engel A, Agre P (1999) Cellular and molecular biology of the aquaporin water channels. Annu Rev Biochem 68:425–458

Breed J, Sankararamakrishnan R, Kerr ID, Sansom MSP (1996) Molecular dynamics simulations of water within models of transbilayer pores. Biophys J 70:1643–1661

Burykin, A., Warshel, A. (2003). What really prevents proton transport through aquaporin? Charge self-energy versus proton wire proposals. Biophys J 85:3696–3706

Capener CE, Sansom MSP (2002) MD Simulations of a K channel model—sensitivity to changes in ions, waters and membrane environment. J Phys Chem B 106:4543–4551

Carloni P, Rothlisberger U, Parrinello M (2002) The role and perspective of ab initio molecular dynamics in the study of biological systems. Acc Chem Res 35:455–464

Chang G, Roth CB (2001) Structure of MsbA from *E. coli:* a homolog of the multidrug resistance ATP binding cassette (ABC) transporters. Science 293:1793–1800

Chang G, Spencer RH, Lee AT, Barclay MT, Rees DC (1998) Structure of the MscL homolog from *Mycobacterium tuberculosis*: a gated mechanosensitive ion channel. Science 282:2220–2226

Darden T, York D, Pedersen L (1993) Particle mesh Ewald—an N.log(N) method for Ewald sums in large systems. J Chem Phys 98:10089–10092

Davis ME, Madura JD, Luty BA, McCammon JA (1991) Electrostatics and diffusion of molecules in solution: simulations with the University of Houston Brownian dynamics program. Comput Phys Comm 62:187–197

de Groot BL, Grubmuller H (2001) Water permeation across biological membranes: Mechanism and dynamics of aquaporin-1 and GlpF. Science 294:2353–2357

de Groot BL, Engel A, Grubmüller H (2001) A refined structure of human aquaporin-1. FEBS Lett 504:206–211

de Groot BL, Frigato T, Helms V, Grubmuller H (2003) The mechanism of proton exclusion in the aquaporin-1 water channel. J Mol Biol 333:279–293

Doyle DA, Cabral JM, Pfuetzner RA, Kuo A, Gulbis JM, Cohen SL, Cahit BT, MacKinnon R (1998) The structure of the potassium channel: molecular basis of K^+ conduction and selectivity. Science 280:69–77

Dutzler R, Campbell EB, Cadene M, Chait BT, MacKinnon R (2002) X-ray structure of a ClC chloride channel at 3.0 Å reveals the molecular basis of anion selectivity. Nature 415:287–294

Fiser A, Kinh Gian Do R, Sali A (2000) Modeling of loops in protein structures. Prot Sci 9:1753–1773

Forrest LR, Kukol A, Arkin IT, Tieleman DP, Sansom MSP (2000) Exploring models of the Influenza A M2 channel:- MD Simulations in a lipid bilayer. Biophys J 78:55–69

Fu D, Libson A, Miercke LJW, Weitzman C, Nollert P, Krucinski J, Stroud RM (2000) Structure of a glycerol-conducting channel and the basis of its selectivity. Science 290:481–486

Fujiyoshi Y, Mitsuoka K, de Groot BL, Philippsen A, Grubmuller H, Agre P, Engel A (2002) Structure and function of water channels. Curr Opin Struct Biol 12:509–515

Guidoni L, Carloni P (2002) Potassium permeation through the KcsA channel: a density functional study. Biochim Biophys Acta 1563:1–6

Hein J, Wiuf C, Knudsen B, Moller MB, Wibling G (2000) Statistical alignment: computational properties, homology testing and goodness-of-fit. J Mol Biol 302:265–279

Hermans J, Berendsen HJC, van Gunsteren WF, Postma JPM (1984) A consistent empirical potential for water-protein interactions. Biopolymers 23:1513–1518

Hess B, Bekker H, Berendsen HJC, Fraaije JGEM (1997) LINCS: A linear constraint solver for molecular simulations. J Comp Chem 18:1463–1472

Heymann JB, Engel A (2000) Structural clues in the sequences of the aquaporins. J Mol Biol 295:1039–1053

Hohmann S, Bill RM, Kayingo G, Prior BA (2000) Microbial MIP channels. Trends Microbiol 8:33–38

Huang Y, Lemieux MJ, Song J, Auer M, Wang DN (2003) Structure and mechanism of the glycerol-3-phosphate transporter from *Escherichia coli*. Science 301:616–620

Humphrey W, Dalke A, Schulten K (1996) VMD—visual molecular dynamics. J Mol Graph 14:33–38

Jensen MO, Tajkhorshid E, Schulten K (2001) The mechanism of glycerol conduction in aquaglyceroporins. Structure 9:1083–1093

Jiang Y, Lee A, Chen J, Cadene M, Chait BT, MacKinnon R (2002) Crystal structure and mechanism of a calcium-gated potassium channel. Nature 417:515–522

Jiang Y, Lee A, Chen J, Ruta V, Cadene M, Chait BT, Mackinnon R (2003) X-ray structure of a voltage-dependent K^+ channel. Nature 423:33–41

Jung JS, Preston GM, Smith BL, Guggino WB, Agre P (1994) Molecular structure of the water channel through aquaporin CHIP: the hourglass model. J Biol Chem 269:14648–14654

Kabsch W, Sander C (1983) Dictionary of protein secondary structure:- pattern-recognition of hydrogen-bonded and geometrical features. Biopolymers 22:2577–2637

Kraulis PJ (1991) MOLSCRIPT: a program to produce both detailed and schematic plots of protein structures. J Appl Cryst 24:946–950

Kuo A, Gulbis JM, Antcliff JF, Rahman T, Lowe ED, Zimmer J, Cuthbertson J, Ashcroft FM, Ezaki T, Doyle DA (2003) Crystal structure of the potassium channel KirBac1.1 in the closed state. Science 330:1921–1926

Laskowski RA, Macarthur MW, Moss DS, Thornton JM (1993) Procheck—a program to check the stereochemical quality of protein structures. J Appl Cryst 26:283–291

Law RJ, Forrest LR, Ranatunga KM, La Rocca P, Tieleman DP, Sansom MSP (2000) Structure and dynamics of the pore-lining helix of the nicotinic receptor: MD simulations in water, lipid bilayers and transbilayer bundles. Proteins Struct Funct Genet 39:47–55

Law RJ, Tieleman DP, Sansom MSP (2003) Pores formed by the nicotinic receptor M2δ peptide: a molecular dynamics simulation study. Biophys J 84:14–27

Locher KP, Lee AT, Rees DC (2002) The *E. coli* BtuCD structure: a framework for ABC transporter architecture and mechanism. Science 296:1091–1098

Luecke H, Schobert B, Richter HT, Cartailler JP, Lanyi JK (1999) Structure of bacteriorhodopsin at 1.55 angstrom resolution. J Mol Biol 291:899–911

Murata K, Mitsuoaka K, Hirai T, Walz T, Agre P, Heymann JB, Engel A, Fujiyoshi Y (2000) Structural determinants of water permeation through aquaporin-1. Nature 407:599–605

Nielsen JE, Vriend G (2001) Optimizing the hydrogen-bond network in Poisson-Boltzmann equation-based pK_A calculations. Proteins Struct Funct Genet 43:403–412

Oliva B, Bates PA, Querol E, Avilés FX, Sternberg MJE (1997) An automated classification of the structure of protein loops. J Mol Biol 266:814–430

Park JH, Saier MH (1996) Phylogenetic characterization of the MIP family of transmembrane channel proteins. J Membr Biol 153:171–180

Pomes R, Roux B (1996) Structure and dynamics of a proton wire: a theoretical study of H^+ translocation along the single-file water chain in the gramicidin A channel. Biophys J 71:19–39

Pomes R, Roux B (2002) Molecular mechanism of H^+ conduction in the single-file water chain of the gramicidin channel. Biophys J 82:2304–2316

Pontius J, Richelle J, Wodak S (1996) Deviations from standard atomic volumes as a quality measure for protein crystal structures. J Mol Biol 264:121–136

Preston GM, Jung JS, Guggino WB, Agre P (1993) The mercury sensitive residue at cys-189 in CHIP28 protein. Science 256:385–387

Ren G, Reddy VS, Cheng A, Melnyk P, Mitra AK (2001) Visualization of a water-selective pore by electron crystallography in vitreous ice. Proc Natl Acad Sci USA 98:1398–1403

Resat H, Mezei M (1996) Grand canonical ensemble Monte Carlo simulation of the dCpG/proflavine crystal hydrate. Biophys J 71:1179–1190

Rodriguez R, Chinea G, Lopez N, Pons T, Vriend G (1998) Homology modelling, model and software evaluation: three related sources. CABIOS 14:523–528

Roux B (1997) Influence of the membrane potential on the free energy of an intrinsic protein. Biophys J 73:2980–2989

Roux B (1999) Statistical mechanical equilibrium theory of selective ion channels. Biophys J 77:139–153

Saiz L, Klein ML (2002) Electrostatic interactions in a neutral model phospholipid bilayer by molecular dynamics simulations. J Chem Phys 116:3052–3057

Sali A, Blundell TL (1993) Comparative protein modeling by satisfaction of spatial restraints. J Mol Biol 234:779–815

Sayle RA, Milner-White EJ (1995) RasMol: biomolecular graphics for all. Trends Biochem Sci 20:374–376

Schmitt UW, Voth GA (1998) Multistate empirical valence bond model for proton transport in water. J Phys Chem B 102:5547–5551

Shrivastava IH, Sansom MSP (2000) Simulations of ion permeation through a potassium channel: molecular dynamics of KcsA in a phospholipid bilayer. Biophys J 78:557–570

Smart OS, Goodfellow JM, Wallace BA (1993) The pore dimensions of gramicidin A. Biophys J 65:2455–2460

Smart OS, Neduvelil JG, Wang X, Wallace BA, Sansom MSP (1996) Hole: A program for the analysis of the pore dimensions of ion channel structural models. J Mol Graph 14:354–360

Sui HX, Han BG, Lee JK, Walian P, Jap BK (2001) Structural basis of water-specific transport through the AQP1 water channel. Nature 414:872–878

Tajkhorshid E, Nollert P, Jensen MO, Miercke LJW, O'Connell J, Stroud RM, Schulten K (2002) Control of the selectivity of the aquaporin water channel family by global orientational tuning. Science 296:525–530

Tate CG (2001) Overexpression of mammalian integral membrane proteins for structural studies. FEBS Lett 504:94–98

Tieleman DP, Berendsen HJC, Sansom MSP (1999) An alamethicin channel in a lipid bilayer: molecular dynamics simulations. Biophys J 76:1757–1769

Tieleman DP, Berendsen HJC, Sansom MSP (2001a) Voltage-dependent insertion of alamethicin at phospholipid/water and octane/water interfaces. Biophys J 80:331–346

Tieleman DP, Biggin PC, Smith GR, Sansom MSP (2001b) Simulation approaches to ion channel structure-function relationships. Q Rev Biophys 34:473–561

Tieleman DP, Hess B, Sansom MSP (2002) Analysis and evaluation of channel models: simulations of alamethicin. Biophys J 83:2393–3407

Tobias DJ (2001) Electrostatics calculations: recent methodological advances and applications to membranes. Curr Opin Struct Biol 11:253–261

Tosatto SCE, Bindewald E, Hesser J, Manner R (2002) A divide and conquer approach to fast loop modeling. Prot Eng 15:279–286

van Gunsteren WF, Kruger P, Billeter SR, Mark AE, Eising AA, Scott WRP, Huneberger PH, Tironi IG (1996) Biomolecular simulation: The GROMOS96 manual and user guide. Biomos and Hochschulverlag AG an der ETH Zurich, Zurich

Verbavatz JM, Brown D, Sabolic I, Valenti G, Ausiello DA, VanHoek AN, Ma T, Verkman AS (1993) Tetrameric assembly of CHIP28 water channels in liposomes and cell membranes: a freeze-fracture study. J Cell Biol 123:605–618

Wu Y, Voth G (2002) Computer simulation studies of proton transport in a synthetic ion channel. Biophys J 82:1016

Zhou Y, Morais-Cabral JH, Kaufman A, MacKinnon R (2001) Chemistry of ion coordination and hydration revealed by a K^+ channel-Fab complex at 2.0 Å resolution. Nature 414:43–48

Zhu FQ, Tajkhorshid E, Schulten K (2001) Molecular dynamics study of aquaporin-1 water channel in a lipid bilayer. FEBS Lett 504:212–218